J. Synchrotron Rad. (1997). **4**, 117–124

X-ray Optics Developments at the APS for the Third Generation of High-Energy Synchrotron Radiation Sources

Dennis M. Mills

Advanced Photon Source, Argonne National Laboratory, 9700 South Cass Avenue, Argonne, IL 60439, USA. E-mail: dmm@anlaps.aps.anl.gov

(*Received 6 September 1996; accepted 18 December 1996*)

Third-generation hard-X-ray synchrotron radiation sources simultaneously provide both a need and an opportunity for the development of new short-wavelength optical components. The high power and power densities of the insertion-device-produced X-ray beams have forced researchers to consider what may seem like exotic approaches, such as cryogenically cooled silicon and highly perfect diamond crystals, to mitigate thermal distortions in the first optical components. Once the power has been successfully filtered while maintaining the high beam brilliance, additional specialized optical components can be inserted into the monochromatic beam that take advantage of that brilliance. This paper reviews the performance of such optical components that have been designed, fabricated and tested at the Advanced Photon Source, starting with high-heat-load components and followed by examples of several specialized devices, such as an meV resolution (in-line) monochromator, a high-energy X-ray phase retarder and a phase-zone plate with submicrometer focusing capability.

Keywords: X-ray optics; high-heat-load optics; monochromators; phase-zone plates; polarization; meV resolution.

1. Introduction

The third generation of hard X-ray synchrotron radiation sources that have recently become operational in Europe and the United States, and will soon become operational in Japan, provide simultaneously new technical challenges and scientific opportunities for the designers of short-wavelength X-ray optical components. X-ray beams generated by undulators installed in the straight sections of these new storage rings not only have very high levels of brilliance [typically 10^{18}–10^{19} photons s^{-1} (0.1% bandwidth)$^{-1}$ mm^{-2} $mrad^{-2}$] but also very high total power levels (kilowatts) and power densities (hundreds of kilowatts per $mrad^2$) associated with them. A summary of some of the latest experimental results that have been obtained at the Advanced Photon Source (APS) in the development and testing of both high-heat-load optics and novel X-ray optical components used downstream of the monochromator will be described here. [For a recent overview of optics performance at the European Synchrotron Radiation Facility (ESRF), see Freund (1995*a*).]

2. High-heat-load optics

A variety of approaches have been explored by the APS staff to mitigate the thermal distortion effects in optics exposed directly to the beam from the undulator, which, at 100 mA and closed gap, generates power densities in excess of 150 W mm^{-2} at 30 m from the source (a typical location for the monochromator). For single-crystal-monochromator optics, we have had the best results with cryogenically cooled silicon and room-temperature synthetic diamond components. Neither of these two approaches are new, both having been pioneered at the ESRF (Freund, 1995*a*,*b*; Marot, 1995). However, because of the larger total power and higher power densities that occur at the APS, modifications of the ESRF designs were required.

Cryogenically cooled optics for use with high-power synchrotron radiation beams were first suggested in 1985 for mirrors (Rehn, 1985) and in the following year for crystal monochromators (Bilderback, 1986). As was pointed out in those papers, the advantage of operating single-crystal-silicon optical components at cryogenic temperatures is twofold: (1) the thermal conductivity, k, increases by nearly a decade in going from room temperature to liquid-nitrogen temperatures, while (2) the coefficient of thermal expansion, α, decreases from its room-temperature value of 2.3×10^{-6} K^{-1}, going through zero at 125 K, and then remains small and negative near the boiling temperature of liquid nitrogen. (Liquid nitrogen is an inexpensive, inert cryofluid and has been the coolant of choice for cryogenic operation of high-heat-load synchrotron radiation optics.) Lowering the temperature of silicon from room temperature to liquid-nitrogen temperatures improves the so-called figure of merit, k/α, by over 40-fold (see Table 1).

A significant Argonne contribution to this field was the use of internally cooled optics, *i.e.* optics with liquid nitrogen flowing through them rather than in a contact-cooling arrangement in which the liquid nitrogen flows through a heat sink in good thermal contact with the optical component (Knapp, Rogers, Beno, Jennings & Cowan,

Table 1
Thermal properties of monochromator materials.

Material	Thermal conductivity, k (W cm^{-1} K^{-1})	Thermal expansion coefficient, α (K^{-1})	Figure of merit, $\lvert k/\alpha \rvert$
Si (300 K)	1.48	2.3×10^{-6}	1
Si (80 K)	13.4	-0.5×10^{-6}	42
Diamond (300 K)	15–20	0.8×10^{-6}	29–39

1995). The internally cooled approach provides a more effective method for the removal of the power deposited in the optic than does the contact-cooling approach, thereby keeping the optic at an overall lower temperature. The primary technical difficulty to overcome when using this approach was the development of a vacuum-tight seal between the coolant manifold and the optical component that is radiation hard, thermally cyclable, and introduces minimal strains into the crystal. This problem is exacerbated by the fact that the desired thickness of the diffracting crystal was less than 1 mm. A relatively thin crystal was desired so that a large fraction of the incident beam would be transmitted, hence reducing the absorbed power in the component that has to be removed by the liquid nitrogen. (Reducing the absorbed power is an important consideration because the operating temperature range for single-phase flow with liquid nitrogen is only a few Kelvin, after which boiling could occur, a situation to be avoided.)

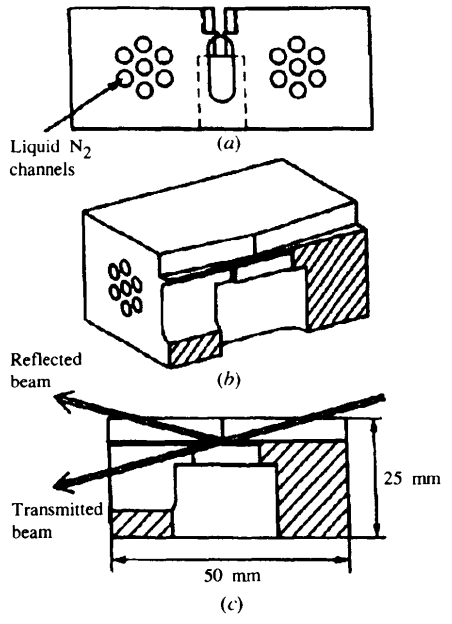

Figure 1
Schematic design and cut-away view of the cryogenically cooled silicon crystal. The end view (*a*) shows the coolant channels and slot, the base of which serves as the diffracting surface for X-rays. The slot has material removed from the underside creating a thin web as shown in (*b*). This thin web permits a portion of the incident beam to be transmitted, thereby reducing the total power absorbed in the crystal (*c*).

A proposed design to overcome these problems was developed (as shown in Fig. 1) in combination with an indium-coated C-ring vacuum seal and special mounting design (Rogers, Mills, Fernandez *et al.*, 1996). As can be seen in Fig. 1, the thin diffracting portion of the crystal is supported on either side by much larger volumes of crystal through which the coolant channels have been machined and where the crystal/manifold seal is made. This crystal design was originally tested at the ESRF under a collaborative agreement between the APS, ESRF and SPring-8 (Rogers *et al.*, 1995; Rogers, Mills, Fernandez *et al.*, 1996), and was recently tested on the Synchrotron Radiation Instrumentation (SRI) Collaborative Access Team (CAT) Sector 1 insertion device beamline at the APS. A summary of the results of the APS tests is shown in Figs. 2 and 3. As can be seen in Fig. 2, very little broadening of the Si (111) rocking curve can be observed even at the highest power densities (lowest energies). The rocking curve of the Si (333) reflection remained approximately constant at 2–3 arcsec as a function of energy, an indication that this width was due to residual strain in the thin part of the crystal from mounting and/or fabrication.

Data in Fig. 3, taken not on the thin portion of the crystal but rather on the top of the thick portion, indicate that the thick portion of the crystal also performed well under thermal load. In fact, the Si (333) reflection is nearly at the theoretical value in the latter geometry, indicating

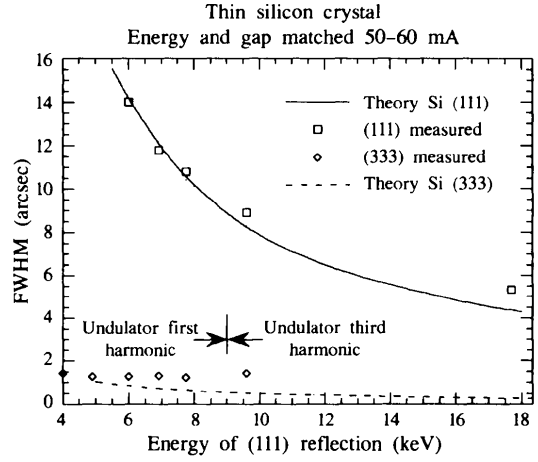

Figure 2
The measured FWHMs of the rocking curves as a function of the X-ray energy diffracted from the Si (111) planes are plotted (squares) along with the solid line representing the theoretical values. Data collected at less than 9 keV were taken using the first harmonic radiation from the undulator, while data collected above 10 keV were taken using the third harmonic from the undulator radiation. No data were taken below 6 keV due to absorption in the commissioning filter/window assembly. Also shown is the FWHM of the Si (333) reflection [taken simultaneously with the Si (111) data] plotted as a function of the X-ray energy from the (111) planes (diamonds). Hence the energy of the X-rays scattered from the (333) planes is three times the displayed abscissa values. The near-constant value of about 1.5 arcsec for the (333) width is indicative of residual strains in the system due to mounting and/or fabrication.

that both the thermal strain and mounting/fabrication strains are below the arcsecond level (Rogers, Mills, Lee, Fernandez & Graber, 1996). These tests were conducted with a commissioning filter/Be window assembly upstream of the monochromator that removed nearly all of the low-energy photons. (The window/filter combination removes about half the flux at 8 keV and reduces the total power density by 14–15% with the undulator gap fully closed, *i.e.* at 11 mm.) In the near future, the effect of this additional power on the monochromator with the window assembly removed will be examined. Also planned are experiments to measure the diffracted beam brilliance from the monochromator system and tests of a reliquefying system for the shell side of the liquid-nitrogen cooling loop. Additional technical details on the APS cryogenic cooling program can be found in Rogers, Mills & Assoufid (1994) and Mills (1996).

Another monochromator design capable of withstanding the thermal loads generated by the APS insertion devices uses synthetic single-crystal diamonds. Single-crystal diamond has approximately the same figure of merit at room temperature as silicon at liquid-nitrogen temperature (see Table 1) but has the added advantage of a lower atomic number compared to silicon (6 for carbon as compared to 14 for silicon), and therefore absorbs considerably less power for a given thickness. The disadvantage of diamond, besides the obvious one of obtaining large perfect single crystals, is that the wavelength-integrated reflectivity of the (111) diamond reflection is about half that of silicon (111). [For an overview of the diffraction properties of diamond, see Blasdell, Assoufid & Mills (1995).]

Nonetheless, because diamonds do not require the complicated cryogenic cooling systems of silicon monochromators, have excellent reflectivity (albeit over a smaller angular or energy range), and can in principle be used in tandem (the transmitted beam can be used as the incident beam for other monochromators further downstream), they are an appealing option for some users of third-generation hard-X-ray sources. Recently, tests of a double-crystal monochromator have been undertaken in which both the first and second crystals are high-quality synthetic diamonds. Fig. 4 shows the mounting scheme employed for the first crystal of the double-diamond monochromator. Good thermal contact between the diamond and the water-cooled substrate is ensured by a thin layer of liquid gallium (80%)/indium (20%) alloy between the diamond and substrate, a technique used a decade ago for silicon crystals (Bilderback, Mills, Batterman & Henderson, 1986) and successfully adapted for use with diamonds at the ESRF (Freund, 1995*b*). The liquid metal not only provides for

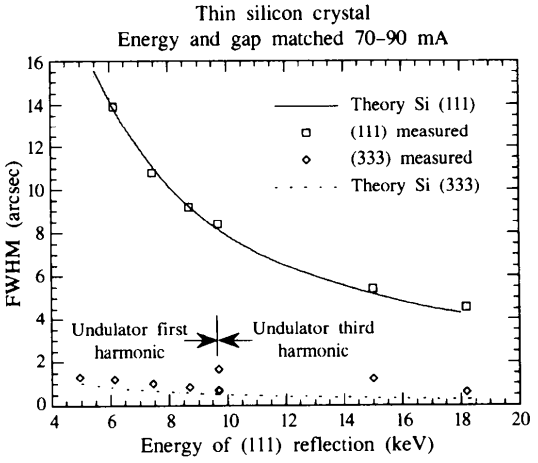

Figure 3
The measured FWHMs of the rocking curves as a function of the X-ray energy diffracted from the Si (111) planes are plotted (squares) along with the solid line representing the theoretical values. Also shown is the FWHM of the Si (333) reflection [taken simultaneously with the Si (111) data] plotted as a function of the X-ray energy from the (111) planes (diamonds). The energy of the X-rays scattered from the (333) planes is three times the displayed abscissa values. Data collected at less than 9 keV were taken using the first harmonic radiation from the undulator, while data collected above 10 keV were taken using the undulator third-harmonic radiation. At about 9.6 keV, the tuning curves for the first and third harmonics of the undulator cross, and here data were taken at both the first and third harmonics. The results are identical for the (111) reflection, but, in the (333) data at 9.6 keV, one of the data points is higher, corresponding to the closed undulator gap (9.6 keV in the third harmonic), and a lower point corresponds to the open undulator gap (9.6 keV in the first harmonic). No data were taken below 6 keV due to absorption in the commissioning filter/window assembly.

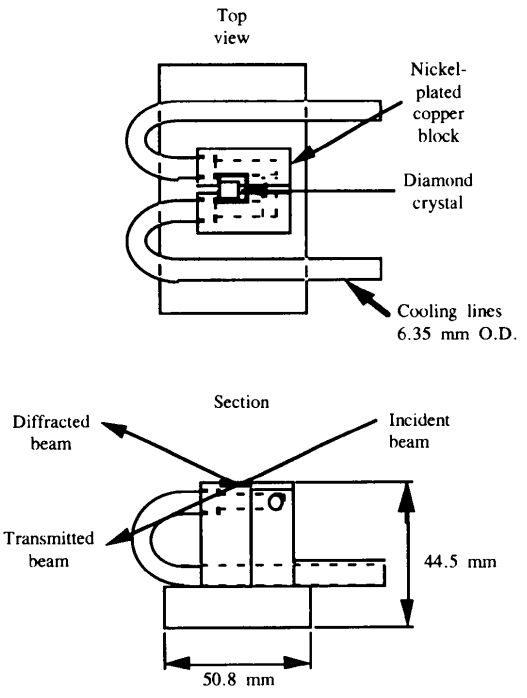

Figure 4
Diamond mounting scheme. The support for the synthetic diamond is a nickel-plated water-cooled copper heat sink with a slot though which the power transmitted by the diamond can pass. A thin layer of liquid In/Ga between the diamond and the cooled heat sink provides both good thermal contact of the diamond to the heat sink and a strain-free method of attaching the diamond to the heat sink (*via* the surface tension of the In/Ga alloy). The copper heat sink is plated with nickel to prevent the gallium from attacking the copper.

good thermal contact but also holds the diamond on the substrate through surface tension.

Fig. 5 is a summary of the experimental results thus far obtained. Although encouraging from a thermal point of view, namely no thermal distortions could be detected, the reproducibility of the data is not nearly as good as that from the silicon. This is due in part to non-perfect diamonds, and so results were dependent on the location of the X-ray beam on the diamond crystals. Comparisons of the flux from the diamond and silicon indicate that the estimate of about a factor of two decrease in flux in the diamond, as compared with silicon, is indeed the case with measured values of the flux ratio of silicon (111) to diamond (111) ranging from 1.4 to 1.9 in the 6–10 keV range (Fernandez & Lee, 1996).

3. In-line monochromators with meV resolution

High-energy-resolution monochromators are a critical ingredient in state-of-the-art inelastic scattering and nuclear resonant scattering beamlines. In these photon-hungry experiments, it is necessary to reduce the energy bandwidth of the beam from the high-heat-load monochromator from a few eV to the required few meV level with very high efficiency. A variety of approaches to produce meV beams have been attempted, including crystals in (+*n*, −*n*, −*n*, +*n*) dispersive arrangements (Faigel *et al.*, 1987) and scattering at Bragg angles very near 90° (Graeff & Materlik, 1982). The former approach has suffered from loss of throughput because of the mismatch between the angular acceptance of the optics and the angular divergence of the X-ray beam, while the latter operates at only discrete X-ray energies that satisfy Bragg's law in the backscattering geometry for some (*hkl*) reflection and necessitates that the beam from the low-resolution monochromator passes in close proximity to the sample on its way to the high-resolution backscattering monochromator.

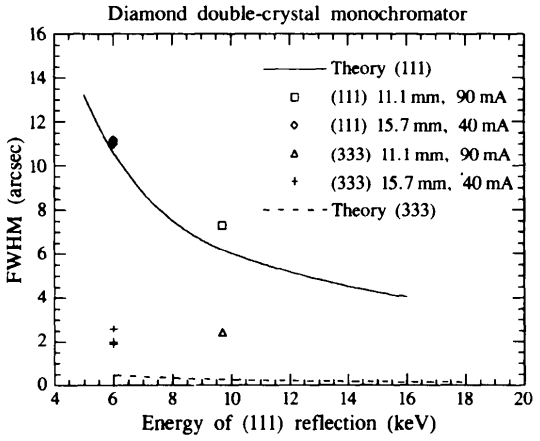

Figure 5
The measured FWHMs of the rocking curves as a function of the X-ray energy diffracted from the (111) planes of diamond are plotted along with the solid line representing the theoretical values. Also shown is the FWHM of the (333) diamond reflection [taken simultaneously with the Si (111) data] plotted as a function of the X-ray energy from the (111) planes. Hence the energy of the X-rays scattered from the (333) planes is three times the displayed abscissa values. Because of the imperfect nature of the diamonds, the experimentally determined FWHM is slightly larger than theory. The spread in the data is primarily due to diffraction from different areas of the diamonds and not to thermal effects. For example, the (333) datum point at 9.6 keV with a FWHM of about 2.5 arcsec was collected at a value of the current twice that of the (333) datum with a FWHM of 3.8 arcsec.

Ishikawa and co-workers (Ishikawa *et al.*, 1992) proposed a new approach, the nested channel cut, that would produce an meV resolution beam with a high throughput over large energy ranges by manipulating the angular divergence of the beam and the angular acceptance of the crystal through asymmetrically cut crystals in an (+*n*, +*m*, −*m*, −*n*) configuration. An asymmetric geometry on the first reflection of the 'outer channel-cut' (*n*) crystal increases the acceptance angle (over that of a symmetrical geometry) and provides a better match for the incident beam divergence while simultaneously providing a highly collimated diffracted beam on the output side to match the angular acceptance of the first reflection of the 'inner channel-cut' (*m*) crystal. The 'inner channel cut' then selects the desired energy width. The second reflection from each of the two channel cuts then replicates the incident beam direction and vertical phase space (*i.e.* size and divergence). This so-called in-line arrangement should not only deliver flux levels comparable with those delivered by the backscattering geometry but should provide much greater flexibility, particularly in its tunability. Energy tuning (over several hundred meV) in the backscattering geometry is achieved by heating or cooling the crystal and changing the *d* spacing and therefore the diffracted energy (since the backscattering angle is fixed). This is a somewhat cumbersome approach and does not allow rapid changes between energies. Energy tuning of the in-line nested monochromator arrangement is simply a matter of changing the Bragg angle of the inner channel cut.

Fig. 6 shows a schematic diagram of a nested channel-cut monochromator that was developed to operate near 14.4 keV for the nuclear resonant scattering program. The operation of the high-resolution nested monochromator is best understood by looking at the corresponding Dumond

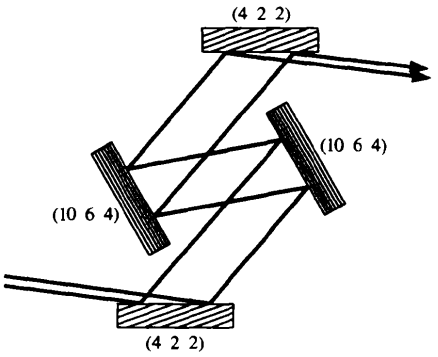

Figure 6
Schematic diagram of the nested crystal monochromator showing the asymmetrically cut (422) outer channel cut and the symmetrically cut (10 6 4) inner channel cut.

diagram shown in Fig. 7 for a 14.4 keV beam in which the n reflection is from the (422) planes and the m reflection from the (10 6 4) planes (Mooney, Toellner, Sturhahn, Alp & Shastri, 1994). [Similar devices have also been produced for 24.8 keV beams using (333) and (555) channel cuts.] A beam with a resolution of 5 meV has been obtained on the Sector 3 insertion device beamline with excellent throughput. Very recently, a beam with an FWHM of less than 1 meV has been produced using a slight variation on this approach [a two-crystal non-in-line arrangement (Toellner & Alp, 1996)]. At wavelengths near 1 Å, this corresponds to a temporal or longitudinal coherence length, $l_c = \lambda^2/\Delta\lambda$, of 1 mm!

4. Dual-polarization high-energy X-ray phase retarders

The production and manipulation of X-ray polarization states by crystal optics has been an ongoing program at the APS. It is our belief that the use of crystal optics for the production of highly polarized hard X-ray beams not only can generate beams with a higher degree of circular polarization than specialized insertion devices but offers opportunities of greater flexibility at a substantially lower cost. The primary motivation for the production of high-energy circularly polarized X-ray beams is for magnetic Compton scattering, although they may have applications in elastic scattering experiments as well.

High-energy circularly polarized X-rays (or any other polarization state for that matter) can be generated by taking advantage of the slight differences in the wavevectors associated with the σ- and π-polarized wavefields that occur near the Bragg condition. When the normal to the atomic scattering planes is oriented at 45° with respect to the (linear) polarization vector of the incident radiation, then equi-amplitude π and σ wavefields will be generated. For a crystal in the Laue geometry with a fixed thickness, a $(2n - 1)\pi/2$ phase shift (where n is an integer) between the σ and π wavefields of a given branch of the dispersion surface will develop for specific X-ray energies, and circularly polarized X-rays can be generated. Because the β branch (anomalously high absorption) of the dispersion curve has a 180° phase shift relative to the α branch (anomalously low absorption), the effect will be nullified if both branches are allowed to propagate through the crystal and recombine at the exit surface. If, however, the material and thickness are chosen such that only the wavefields associated with the α branch are transmitted, then the polarization of the output beam can be more readily manipulated. Because the value of the phase shift varies across the reflectivity curve, these phase retarders should perform much better with highly collimated beams, such as those produced by undulators on third-generation sources, than on bending-magnet or wiggler beamlines. The first attempts at producing high-energy (>50 keV) circularly polarized X-rays using this approach were made using a silicon phase retarder (Mills, 1988),† but it was realized that a higher atomic number material would be more effective (to completely absorb the β branch of the dispersion curve), and germanium retarders were developed that provide a much higher degree of circular polarization (Yahnke, Srajer, Haeffner, Mills & Assoufid, 1994).

To extract the magnetic portion of the total (electronic plus magnetic) scattering in ferromagnetic and ferrimagnetic samples, spin-flipping techniques, in which an externally applied field is used to flip the spin direction of the sample, can be used in conjunction with circularly polarized X-rays. Flipping the spin changes the sign of the first-order magnetic term but leaves the charge term unchanged. By subtracting data sets taken in the two spin configurations, the electronic portion of the scattering is removed, leaving only the magnetic contribution. Spin-direction reversal works well with relatively soft ferromagnetic samples, but such switching is not possible with all materials and/or experimental geometries.

The same result can be achieved by leaving the spins fixed and changing the handedness of the circularly polarized X-rays. The ability to readily change the handedness of the polarization opens up a much wider class of materials in various environmental cells (cryostats, furnaces *etc.*) to be explored with magnetic X-ray scattering techniques. Therefore, sources that are capable of providing radiation of both handedness are very desirable. Although it was in principle possible to change the handedness of the radiation in the first generation of high-energy phase retarders, this process was not totally satisfactory. A method for improved helicity reversal was suggested by Hirano and collaborators (Hirano, Ishikawa, Nakamura, Mozutani & Kikuta, 1994)

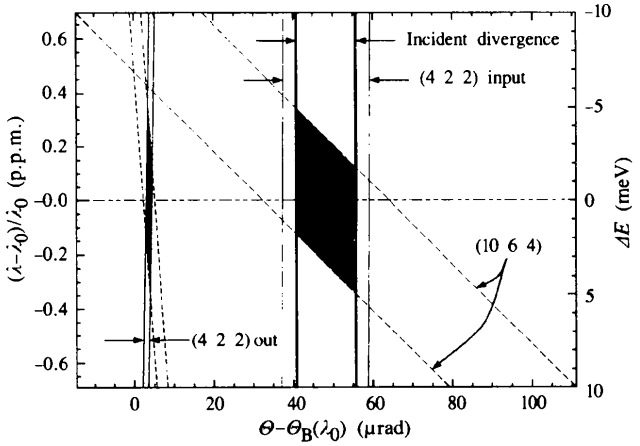

Figure 7
The Dumond diagram for a nested crystal monochromator. The 442 crystal is asymmetrically cut to accept the full incident beam divergence (bold lines), as indicated by the nearly vertical lines in the center of the diagram. The output of the 442 reflection is shown with the acceptance of the (10 6 4) planes (dashed lines) near the zero on the $\Delta\Theta$ axis, the overlap indicated by the shaded area. For clarity, the overlap area and the Darwin width of the (10 6 4) planes have also been mapped onto the (422) input.

† Note there are two corrections to this paper: equation (3) should read $y = [(\Delta\Theta)\sin(2\Theta)\pi V]/(r_e\lambda^2|F_{\mathbf{H}}|)$, and equation (4) should read $Z_{\pi,\sigma} = [(r_e\lambda|F_{\mathbf{H}}||P|)/(2\pi V)]\{(y^2 + 1)^{1/2} - [y^2 + \cos(2\Theta)]^{1/2}\}$.

but suffered from a limited throughput. In the latest design developed at the APS, the Hirano concept has been extended to retain a high throughput by simultaneously producing two circularly polarized radiation beams, of opposite handedness, displaced in space from one another.

A schematic diagram of this new phase retarder design is shown in Fig. 8. The Bragg reflection acts as a beam splitter, sending two monochromatic beams (from the $\langle 110 \rangle$ and $\langle 1\bar{1}0 \rangle$ family of planes) to the equivalent planes in the Laue portion of the phase retarder, where the phase shifting is accomplished to produce the circularly polarized X-rays. If the plane containing the $\langle 1\bar{1}0 \rangle$ and $\langle 110 \rangle$ reciprocal lattice vectors is normal to the plane of diffraction from the $\langle 100 \rangle$ planes, then a condition for multiple diffraction is satisfied for all three reflections ($\langle 1\bar{1}0 \rangle$, $\langle 110 \rangle$ and $\langle 100 \rangle$); a condition that can alter the desired polarization effect. The multiple-beam condition can be eliminated by rotating about the $\langle 100 \rangle$ vector, which breaks the symmetry of the geometry. (The angles between the incident beam and the two sets of $\{110\}$-type planes are no longer equal, and the energies of the $\langle 1\bar{1}0 \rangle$ and $\langle 110 \rangle$ reflections occur at slightly different values.) The X-ray polarization incident on the sample is changed by a small translation (millimeters) of the sample from one beam to the other.

This device was recently tested on the Sector 1 undulator beamline of SRI CAT. The degree of circular polarization of the beams was measured at a series of energies, and measurements were made on both beams at an energy at which the degree of circular polarization was calculated to be near unity ($P_c = \pm 1$). The results of these measurements are shown in Fig. 9. The high degree of circular polarization of both left and right handedness that can be produced with this new type of phase retarder will open up magnetic Compton scattering to a host of new magnetic materials in which switching of the spin direction is impossible.

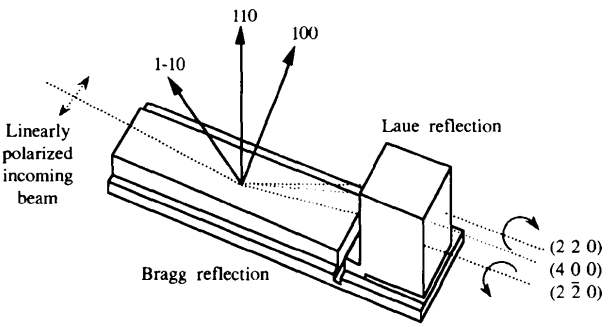

Figure 8
Schematic diagram of the dual-polarization phase retarder. The entire device consists of a monolithic Bragg/Laue crystal pair for the improved stability required for operation at high energies. The Bragg crystal serves as a monochromator and beam splitter, while the polarization manipulation is performed in the Laue crystal. The two output beams, separated by several millimeters, have opposite helicities.

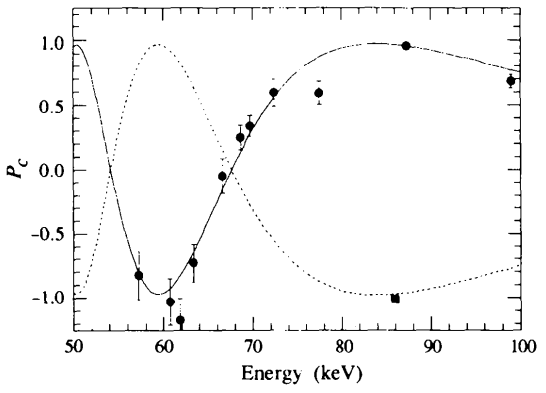

Figure 9
Experimental results of the dual-beam phase plate. The measured and theoretical degree of circular polarization, P_c, as a function of energy for the (220) reflection (circles and solid line) and the ($2\bar{2}0$) reflection (square and dashed line) for a 14.5 mm-thick germanium phase plate. The maxima (minima) at about 85 keV (60 keV) corresponds to a phase shift of $\pi/2$ ($3\pi/2$). P_c was determined experimentally *via* magnetic Compton scattering from iron.

5. Phase-zone plates

The use of zone plates for the focusing of X-rays is well established in the synchrotron community, especially in the soft X-ray microscopy community (Lai *et al.*, 1992; Kirz, Jacobsen & Howells, 1995). A zone plate is a structure composed of alternating concentric rings of two materials with different (complex) refractive indices. The focusing capability is based on constructive interference of the wavefront modified by passage through the zone plate. The wavefront modification is obtained through the introduction of a relative change in amplitude or phase in the beams emerging from two neighboring zones. A zone plate is called an amplitude zone plate if the focusing results from the different absorption between two neighboring zones. It is called a phase-zone plate if the phase change upon transmission through a zone is the mechanism for the focusing.

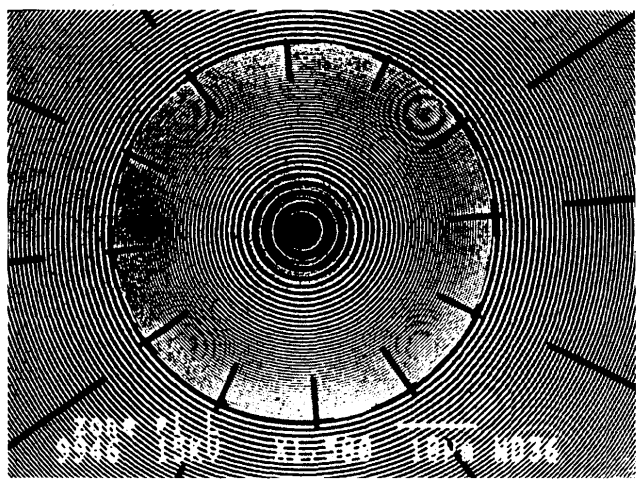

Figure 10
Scanning electron micrograph of the phase-zone plate used at the APS. The width of the outermost zone is 0.15 μm, and the thickness of the zone plate is 1.6 μm.

In general, the size of the focal spot from the zone plate is determined by the width of the outermost ring. Using state-of-the-art lithographic technologies, zones plates with outermost ring widths of less than 30 nm can currently be fabricated. If illuminated with an X-ray beam whose spatial coherence length is equal to or greater than the size of the zone plate, a diffraction-limited focus can be obtained. Third-generation sources, such as the APS, can provide the required spatial coherence at appreciable flux levels. (Temporal coherence is also required but only to the extent that $E/\Delta E$ is greater than the number of rings or zones.)

In the soft X-ray region, zone-plate efficiency is limited to about 15% due to photoelectric absorption. For X-ray energies greater than 3 keV, it is in principle possible to produce phase-zone plates with focusing efficiencies close to 40%. In a recent experiment on the Sector 2 insertion device beamline at the APS with a composite zone plate (see Fig. 10) placed behind an Si (111) monochromator (bandwidth $\simeq$ 0.01%), a focal spot size (FWHM) of 0.46 μm in the vertical direction and 1.2 μm in the horizontal direction was obtained at 11.4 keV (see Fig. 11). The focal length of the outer zone plate is three times that of the inner zone plate, which is 5 cm for 8 keV X-rays. This allows the first-order focus from the inner zone plate to coincide with the third-order focus from the outer zone plate. With this zone plate, a photon flux of 4×10^9 photons s^{-1} was obtained at the focus with the storage ring operating at 40 mA (Yun, 1996).

6. Conclusions

In the early planning stages of third-generation synchrotron radiation sources, there were serious concerns as to whether the full brilliance of these sources could ever be brought to the experiment because of thermal degradation of the first optical components. Within the current operational envelope of the two working third-generation hard-X-ray storage rings (ESRF and APS), the initial indications are that this will not be the case. Cryogenically cooled silicon crystals and water-cooled diamond crystals seem capable of handling the currently available beams (although, at this point in time, few careful measurements of beam brilliance after the first high-heat-load components have been made and published). Although high-heat-load optics may seem well in hand, alternative approaches are under active investigation at the various facilities to improve component performance, and the combined effects of increased stored beam current, longer insertion devices, and smaller magnetic gaps that are slated for the future will continue to provide challenges to scientists and engineers working on high-heat-load optical components.

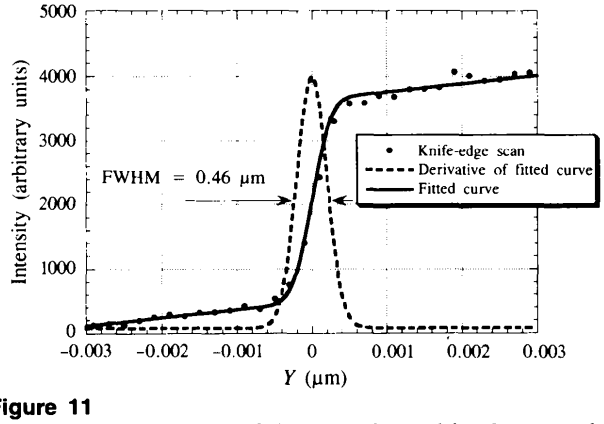

Figure 11
Measurement of the size of the beam focused by the zone plate (E = 11.4 keV, f = 6.7 cm). The focal spot size was characterized using a knife-edge method. A 1 mm-thick Ni film on an Si substrate served as the knife edge and was prepared using a lithographic technique. In the knife-edge scan method, the Ni $K\alpha$ fluorescence signal was recorded when the edge was scanned across the focal spot. By differentiating the intensity as a function of the knife-edge position, we obtained full width half maximum of the focal spot size of 0.46 mm and 1.2 mm for the vertical and horizontal directions, respectively.

Single-crystal optics have been the mainstay of synchrotron radiation optical components in the past and will continue to be important at third-generation sources. Although silicon is certainly the workhorse of single crystals, as pointed out in this paper, good-quality diamond and germanium crystals can play important roles. All of the single-crystal optical components described above were fabricated and/or initially characterized off-line in the APS X-ray Optics Fabrication and Characterization Facility. The importance of such a facility in the development of these and other X-ray optics components cannot be overstated. During the development of the APS and its associated support facilities, provisions were included for an X-ray single-crystal fabrication and characterization laboratory (Krasnicki, 1996), a deposition facility and a metrology laboratory (Bresloff & Mills, 1996). All three of these facilities are now up and running at the APS and provide invaluable support to researchers developing and testing X-ray optical components.

Although single-crystal optics will remain prevalent, man-made X-ray optical components (coated mirrors, multilayers and zone-plate-based optics, capillaries, *etc.*) will play an ever increasing role in the future of X-ray optics development at third-generation sources. High-quality/high-speed deposition systems will be required for the manufacture of some components. Hard X-ray lithographic techniques will also become an important tool for the fabrication of other new X-ray optical components, and the SRI CAT has included a program of deep-etch X-ray lithography to be based on the bending-magnet beamline of Sector 2 for the development of such optical components.

A final, and important, point that needs mention is use of coherent hard-X-ray beams and the development of coherent X-ray optical components, an area only briefly alluded to in this paper. This field will certainly be a growth area in the future. The fabrication capabilities described above, in combination with the high source brilliance achievable from third-generation X-ray sources, will provide researchers with the tools they need to develop and explore the use of coherent X-ray optics in the years to come.

The work described in this overview is due to the effort of many staff members of the Experimental Facilities Division of the Advanced Photon Source. The cryogenically cooled silicon and diamond monochromator experimental team included Shawn Rogers, Patricia Fernandez, Wah-Keat Lee, Tim Graber and Lahsen Assoufid. Work on the in-line nested monochromator described above was undertaken by Ercan Alp, Tom Toellner, Tim Mooney, Wolfgang Sturhahn and Klaus Quast. Contributors to the development and testing of the high-energy X-ray phase retarder were Jonathan Lang, George Srajer, Sarjvit Shastri, Dean Haeffner and Christie Nelson. The zone-plate work was performed by Wenbing Yun, B. Lai, Z. Cai, D. Legnini, E. Gluskin, A. Krasnoperova, Z. Chen, F. Cerinna, E. DiFabrizio and M. Centili. Thanks also go to Ian McNulty for clear explanations on the operations of zone plates. All of the silicon and germanium crystal optical components were fabricated in the APS Optics Fabrication and Characterization lab, run by Felix Krasnicki. We also acknowledge the Harris Diamond Corporation for working with the APS in obtaining the high-quality diamonds used in these tests. This work was supported by the US Department of Energy, BES Materials Sciences, under contract No. W-31-109-ENG-38.

References

Bilderback, D. H. (1986). *Nucl. Instrum. Methods*, **A246**, 434–436.

Bilderback, D. H., Mills, D. M., Batterman, B. W. & Henderson, C. (1986). *Nucl. Instrum. Methods*, **A246**, 428–433.

Blasdell, R. C., Assoufid, L. A. & Mills, D. M. (1995). *Diamond Monochromators for APS Undulator-A Beamlines*. Report ANL/APS/TB-24. Argonne National Laboratory, Argonne, USA.

Bresloff C. & Mills, D. M. (1996). *Rev. Sci. Instrum.* **67**, 3369.

Faigel, G., Siddons, D. P., Hastings, J. B., Haustein, P. E., Grover, J. R., Remeika, J. P. & Cooper, A. S. (1987). *Phys. Rev. Lett.* **58**, 2699–2701.

Fernandez, P. B. & Lee, W.-K. (1996). Private communication.

Freund, A. K. (1995*a*). *SPIE J.* **2515**, 445–457.

Freund, A. K. (1995*b*). *Opt. Eng.* **34**, 432–440.

Graeff, W. & Materlik, G. (1982). *Nucl. Instrum. Methods*, **195**, 97–103.

Hirano, H., Ishikawa, T., Nakamura, I., Mozutani, M. & Kikuta, S. (1994). *Jpn. J. Appl. Phys.* **33**, L689-L692.

Ishikawa, T., Yoshitaka, Y., Izumi, K., Suzuki, C. K., Zhang, X. W., Ando, M. & Kituta, S. (1992). *Rev. Sci. Instrum.* **63**, 1015–1018.

Kirz, J., Jacobsen, C. & Howells, M. (1995). *Q. Rev. Biophys.* **28**, 33–130.

Knapp, G. S., Rogers, C. S., Beno, M. A., Jennings, G. & Cowan, P. L. (1995). *Rev. Sci. Instrum.* **66**, 2138–2140.

Krasnicki, S. (1996). *Rev. Sci. Instrum.* **67**, 3369.

Lai, B., Yun, W., Legnini, D., Xiao, Y., Chrzas, J., Viccaro, P. J., White, V., Bajikar, S., Denton, D., Cerrina, F., Di Fabrizio, E., Gentili, M., Grella, L. & Baciocchi, M. (1992). *Appl. Phys. Lett.* **61**, 1877–1879.

Marot, G. (1995). *Opt. Eng.* **34**, 426–431.

Mills, D. M. (1988). *Nucl. Instrum. Methods*, **A266**, 531–537.

Mills, D. M. (1996). *Rev. Sci. Instrum.* **67**, 3348.

Mooney, T. M., Toellner, T., Sturhahn, W., Alp, E. E. & Shastri, S. D. (1994) *Nucl. Instrum. Methods*, **A347**, 348–351.

Rehn, V. (1985). *SPIE J.* **582**, 238–250.

Rogers, C. S., Mills, D. M. & Assoufid, L. (1994). *The Cryogenic Cooling Program at the Advanced Photon Source*. Report ANL/APS/TB-18. Argonne National Laboratory, Argonne, USA.

Rogers, C. S., Mills, D. M., Fernandez, P. B., Knapp, G. S., Wulff, M., Hanfland, M., Rossat, M., Freund, A., Marot, G., Holmberg, J. & Yamaoka, H. (1996). *Rev. Sci. Instrum.* **67**, 3350.

Rogers, C. S., Mills, D. M., Lee, W.-K., Fernandez, P. B. & Graber, T. (1996). *SPIE J.* **2855**, 170–179.

Rogers, C. S., Mills, D. M., Lee, W.-K., Knapp, G. S., Holmberg, J., Freund, A., Wulff, M., Rossat, M., Hanfland, M. & Yamaoka, H. (1995). *Rev. Sci. Instrum.* **66**, 3494–3499.

Toellner, T. & Alp, E. E. (1996). Private communication.

Yahnke, C. J., Srajer, G., Haeffner, D. R., Mills, D. M. & Assoufid, L. (1994). *Nucl. Instrum. Methods*, **A347**, 128–133.

Yun, W. (1996). Private communication.